catalysts

MDPI

Article

Applying Hydrogenation to Stabilize N-TiO_2 and Enhance Its Visible Light Photocatalytic Activity

Dongqiu Zhao [1], Xiao Tang [2], Xuming Qin [1], Zhenjie Tang [1], Di Yuan [1] and Lin Ju [1,*]

[1] School of Physics and Electrical Engineering, Anyang Normal University, Anyang 455000, China; dqzhao@aynu.edu.cn (D.Z.); xmqin@aynu.edu.cn (X.Q.); zjtang@aynu.edu.cn (Z.T.); yuandi@aynu.edu.cn (D.Y.)
[2] Institute of Materials Physics and Chemistry, College of Science, Nanjing Forestry University, Nanjing 210037, China; xiaotang@njfu.edu.cn
* Correspondence: julin@aynu.edu.cn

Abstract: Up to now, the explanation for the origin of enhanced photocatalytic activity of N doped TiO_2 (N-TiO_2) with H incorporation, which is observed in experiment, is still lacking. In our work, the effects of hydrogenation on the stability and electronic properties of N-TiO_2 have been systematically investigated by first-principles calculations. Our results of the study on stability demonstrate that, both full and part hydrogenation could stabilize N-TiO_2 by largely reducing the formation energy of N doping under Ti-rich conditions. Moreover, the calculated results on the electronic structure show that, for the completely hydrogenated N-TiO_2, band gap becomes slightly larger, which is caused by the full passivation for unpaired electron from N atom. However, for the partially hydrogenated N-TiO_2, due to the interaction between hydrogenated and unhydrogenated N atoms, its valence band maximum shifts to higher energy by 0.32 eV and the valence band states mix with the wide band-gap states, which results in a higher light absorption capacity and carrier separation. Our results not only explain the enhancement of visible light photocatalytic activity experimentally found in N-TiO_2 specimen with H incorporation, but also indicate that, tuning the hydrogenation degree is a hopeful routine to improve the photocatalytic performance of N-TiO_2.

Keywords: hydrogenation; water-splitting; N-TiO_2; photocatalysis

check for updates

Citation: Zhao, D.; Tang, X.; Qin, X.; Tang, Z.; Yuan, D.; Ju, L. Applying Hydrogenation to Stabilize N-TiO_2 and Enhance Its Visible Light Photocatalytic Activity. *Catalysts* **2022**, *12*, 178. https://doi.org/10.3390/catal12020178

Academic Editor: Anna Kubacka

Received: 31 December 2021
Accepted: 27 January 2022
Published: 29 January 2022

Publisher's Note: MDPI stays neutral with regard to jurisdictional claims in published maps and institutional affiliations.

Copyright: © 2022 by the authors. Licensee MDPI, Basel, Switzerland. This article is an open access article distributed under the terms and conditions of the Creative Commons Attribution (CC BY) license (https://creativecommons.org/licenses/by/4.0/).

1. Introduction

Due to the ever-growing energy crisis and environmental pollution problems, the development of clean, environmentally friendly and sustainable alternative energy sources is urgently required. Hydrogen is an ideal alternative energy source for traditional fossil fuels because of its high energy density and low greenhouse gas emission. Since the discovery of "Honda-Fujima" effect [1], photocatalytic water splitting has been considered as an optimal pathway for hydrogen production, which has received extensive attention for decades [2–7]. Efficient and stable photocatalysts plays a key role in improving the efficiency of photocatalytic water splitting. As an originator photocatalyst, anatase titanium dioxide (TiO_2) has attracted a great interest for the application of hydrogen generation [8] and environmental cleanup [9]. Although it possesses strong photocatalytic activity, high physical and chemical stability, and nontoxicity [10], its energy conversion efficiency is extremely low, which is caused by its large band gap (E_g) (~3.2 eV) [11] and high electron-hole recombination rate. The large E_g makes its photo-responsive only to the ultraviolet light (about 5% of the total solar spectrum), great limiting the light utilization rate. Tremendous experimental and theoretical research has demonstrated that, ion doping is an effective way to raise the photocatalytic performance of TiO_2 by lowering its E_g and/or reducing the recombination rate of photogenerated electron-hole pairs [12–20].

For an overall water-splitting photocatalyst, the desirable E_g is about 2.0 eV, and the band edges must straddle the redox potential levels of water [21]. The valence band

maximum (VBM) potential of TiO_2 is far below the water oxidation level, but its conduction band minimum (CBM) is slightly above the hydrogen reduction level [22]. Therefore, the ideal doping pattern is such that VBM is substantially elevated, while CBM remains at the original position. Doping nitrogen atoms to form N-TiO_2 is such an effective approach [23,24] that, it could optimize the VBM of TiO_2 and keep the CBM at the same position [25]. However, due to the high formation energy, the substitutional N doping level is extremely low, which limits the improvement of VBM [26]. The oxygen vacancies (Vo) induced by N doping can compensate for the high formation energy of N-TiO_2. However, the Vo introduced in the bulk TiO_2 is prone to become recombination centers for photogenerated electron-hole pairs, and the visible light photocatalytic activity of N-TiO_2 does not improve with N doping concentration increase [24]. This is contrary to the introduced Vo by N doping on the surface of TiO_2, which can achieve efficient co-catalyst-free photocatalytic activity under less extreme conditions [27]. Therefore, to obtain a higher efficiency, the VBM of bulk N-TiO_2 should be further modified by some other methods.

It has found that, compared to pristine N-TiO_2, the specimen with H incorporation has a better visible light (VL) photocatalytic performance [28]. The N-doping concentration can be increased from 2% to 4.4% when the N-doped TiO_2 was prepared under NH_3 atmosphere [29]. Earlier theoretical calculations proposed that, the enhancement of VL photocatalytic performance was attributed to the narrowed E_g after hydrogenation [28]. Later, another theoretical research suggested that, the hydrogenation did not reduce the E_g of N-TiO_2, instead, it brought in some distortion of local structure near N atoms, which is accounted for the improvement of VL photocatalytic activity [30]. Moreover, some other theoretical results even stated that, the increase of VL photocatalytic efficiency was ascribed to the disappearance of band-gap states, because they found that hydrogenation made the E_g of N-TiO_2 become larger [31,32]. This explanation must be untenable, because band-gap states serve as a springboard for the photoexcitation of electrons in N-TiO_2 [25], without which, the use ratio of visible light is greatly reduced. To sum up the above, the origin of enhanced VL photocatalytic activity of N-TiO_2 with H incorporation was still confusing.

In addition, during the experimental fabrication of N-TiO_2 with H incorporation, normally, due to the complex preparation conditions [29], the N atoms may be hardly completely hydrogenated, so there is often a coexistence of hydrogenated and unhydrogenated N atoms (marked as N_h and N_u for short, respectively). Although, to date, there have been massive configurations for N-TiO_2 with H incorporation studied by density functional theory (DFT) calculations, such as substitutional NH for O, interstitial NH, and $H_{n(1\sim4)}$ occupying Ti or interstitial sites with N doping, etc. [28,30–33]. The study on partially hydrogenated N-TiO_2, which contains N_h and N_u, is still absent. Hence the effect of N_u-N_h interaction on its stability and photocatalytic performance is unclear yet.

In this work, to explore the enhancement of N-TiO_2 photocatalytic activity caused by hydrogenation, we built completely and partially hydrogenated N-TiO_2 models, and studied their morphology, formation energy, electronic structures, and optical properties. Based on the results above, the influence of hydrogenation on the VL photocatalytic activity of N-TiO_2 was further discussed.

2. Calculation Method

The atomic models were built with the DeviceStudio software [34], which also could provide a number of functions for performing visualization, modeling and simulation. The calculations were performed using the ultrasoft pseudopotentials with generalized gradient approximation of the Perdew-Wang 91 as implemented in the CASTEP code [35]. Considering that there is one unpaired electron in pristine and partially hydrogenated N-TiO_2, spin-polarized DFT was employed to study the electronic structures of these systems. Though the E_g calculated with our method normally is smaller than the experimental value, our results still could reflect the relative changes of electronic structures among these samples considered in our study. More information for this could be found in the Supplementary Materials. The Monkhorst-Pack *k*-point sampling [36] for Brillouin zone

integration was generated with a 3 × 7 × 3 grid, and the cutoff energy for the plane wave expansion was 340 eV. The valence atomic configurations were used as $1s^1$ for H, $2s^2 2p^3$ for N, $2s^2 2p^4$ for O, and $3s^2 3p^6 3d^2 4s^2$ for Ti. The imaginary parts of dielectric functions and optical absorption were calculated with 'scissors operator'. Considering that the formation energies, electronic structures, and optical properties are almost independent of the size of the supercells, and the finite-size effects could be ignored [37]. In order to compare with the previous study of the N doping case [25], we also employed the 2 × 1 × 1 TiO_2 supercell, containing 16 O atoms and 8 Ti atoms, to construct the calculated models. The completely hydrogenated N-TiO_2 (symbolized as sample I for short) model was realized by replacing one O atom with an N atom, where H atom was bonded to the N atom and perpendicular to the Ti–O–Ti plane. Similar substitutions were used to build the partially hydrogenated N-TiO_2 (symbolized as sample II for short) configuration, in which two O sites were separately occupied by a N_u and N_h atom.

3. Results and Discussion

3.1. Crystal Structure and Formation Energy

After optimization, the stable configurations for sample I and sample II were plotted in Figure 1, and their lattice parameters remain almost unchanged compared to N-TiO_2 (as listed in Table S1). However, there occur some slight changes for the local structure adjacent to N_h. For instance, the N_h dose not situate in its three-nearest-Ti plane, instead, it moves into the tetrahedral body, which is made of the bonded hydrogen and the three-nearest-Ti. In sample I, the N–H bond length was 1.034 Å. In sample II, it shortens to 1.031 Å, suggesting an enhanced covalent bond between the N ion and the H proton. These N–H bond lengths are comparable to that in an NH_3 molecule (1.05 Å) [30].

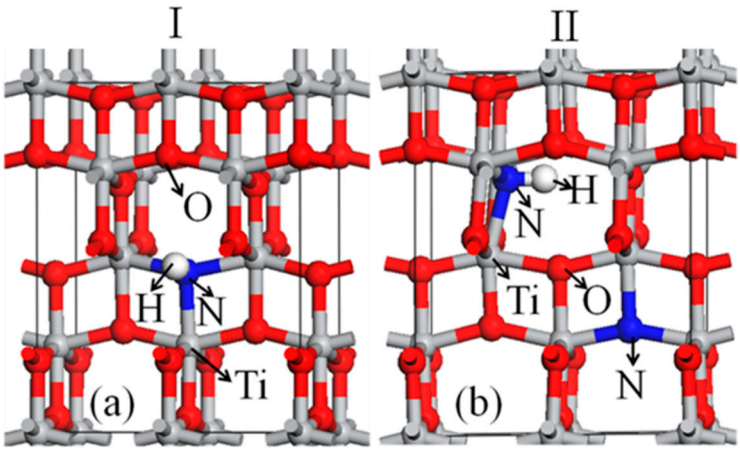


Figure 1. The optimized supercell models for (**a**) completely and (**b**) partially hydrogenated N-TiO_2 marked as samples I and II, respectively; the atomic sites of H (white ball), N (blue ball), O (red ball), and Ti (gray ball) are marked in (**a**) and (**b**), respectively.

To examine the influence of hydrogenation on the stability of these doped systems, we calculate the formation energies E_{form} according to the Equation (1) below [32]:

$$E_{form} = E_{doped} - (E_{pure} + n\mu_N + \mu_H - n\mu_O) \quad (1)$$

in which E_{doped} and E_{pure} are the total energy of the TiO_2 supercell with and without dopant, respectively. The symbol n represents the number of O atoms substituted by N dopants in a supercell, and μ_O, μ_N, and μ_H refer to the chemical potentials of O, N and H, respectively. The formation energy depends on the chemical potentials of the host and dopant atoms. The value of chemical potential μ_O is determined by growth conditions, which is varied from O-rich condition to Ti-rich condition. Under O-rich conditions, μ_O is obtained from the energy of the ground-state of the O_2 molecule ($\mu_O = {}^1/_2\,\mu_{O2}$). And under Ti-rich conditions, μ_O is

calculated from the formula $\mu_{Ti} + 2\mu_O = \mu(TiO_2)$, where μ_{Ti} equals to the energy of one Ti atom in Ti bulk. For dopants, μ_N and μ_H are determined by the energy of the ground-states, namely N_2 and H_2 molecules, ($\mu_N = {}^1/_2\ \mu_{N2,}\ \mu_H = {}^1/_2\ \mu_{H2}$) respectively. The calculated formation energies for N-TiO_2, sample I, and sample II are listed in Table 1, which reveals that, in Ti-rich condition, which is more energetically favorable to form doped systems than O-rich condition, the hydrogenated N-TiO_2 has much lower formation energy than the pristine N-TiO_2, implying that a higher substitutional N doping concentration may be achieved with H incorporation during the experimental fabrication process. Additionally, as displayed in Figure S1, we also considered the configurations with H bonded to O (H–O) and H bonded to Ti (H–Ti). As listed in Tables 1 and S2, the calculated formation energies for the H–O model and the H–Ti model separately are 0.506 eV and 0.654 eV higher than that of sample I, which indicates that the configuration of sample I is the most energetically stable. In other words, during the hydrogenation process, the H atom prefers to bind to the doped N atom instead of O and Ti atoms. Therefore, our work chooses the configurations with H bonded to N.

Table 1. Formation energies (E_{form}, in eV) for N-TiO_2, sample I, and sample II under various growth conditions.

E_{form}	Configuration		
	N-TiO_2	**Sample I**	**Sample II**
$E_{form\ (Ti\text{-}rich)}$	0.023	−2.175	−2.454
$E_{form\ (O\text{-}rich)}$	5.002	2.805	7.504

3.2. Electronic Band Structure and Density of States

As well known to all, the band-gap states, introduced by doping heteroatoms, has an essential impact on electronic properties of base materials, then tunes their photocatalytic behaviors. The shallow band-gap state levels, namely the ones close to the valence band (VB) edge (shallow acceptor level) or conduction band (CB) edge (shallow donor level), are able to facilitate the separation of photoexcited electron-hole pairs because they can capture photoexcited carriers [38,39]. For instance, the shallow acceptor level tends to ensnare photoexcited electrons, which could prevent the electrons from recombining with photogenerated holes, prolonging the life time of photogenerated holes, then accelerating the speed of photooxidation reaction. In addition, the band structure of catalysts plays an important role in extending the lifetime of photogenerated electron-hole pairs. For example, the flatter band leads to heavier carrier effective mass, since the effective mass is inversely proportional to the second derivative of the band energy with respect to momentum. The indirect energy band gap results in indirect transitions, which generally increase the electron-hole lifetime relative to direct transitions [40].

After optimizing the crystalline structures, we calculated their band structures (see Figure 2), total density of states (TDOS) and partial density of states (PDOS) (see Figure 4). As shown in Figures 4 and S3, relative to TiO_2, for each system, the CBM remains almost at the same position, whereas the VBM greatly shifts to a higher energy level, which satisfies the requirement of ideal doping pattern for TiO_2 mentioned before. Moreover, as shown in Figure 2b, in sample I, no acceptor state emerges in the band gap, and the VBM shifts to higher energy by 0.22 eV, which is somewhat smaller than that in N-TiO_2 (0.27 eV, as shown in Figure 2a). Hence, the complete hydrogenation makes the E_g of N-TiO_2 slightly larger, which is consistent with most recent reports [31,32]. In addition, the H 1*s* states extend N 2*p* along with O 2*p* and Ti 3*d* states from −4.54 eV to the lower energy zone (see Figure 4b), which mainly corresponds to the σ bonding states. These results indicate that H implantation forms a strong chemical bond with N, which affects not only the electronic states of N but also some electronic states of Ti and O atoms neighboring to the N atoms.

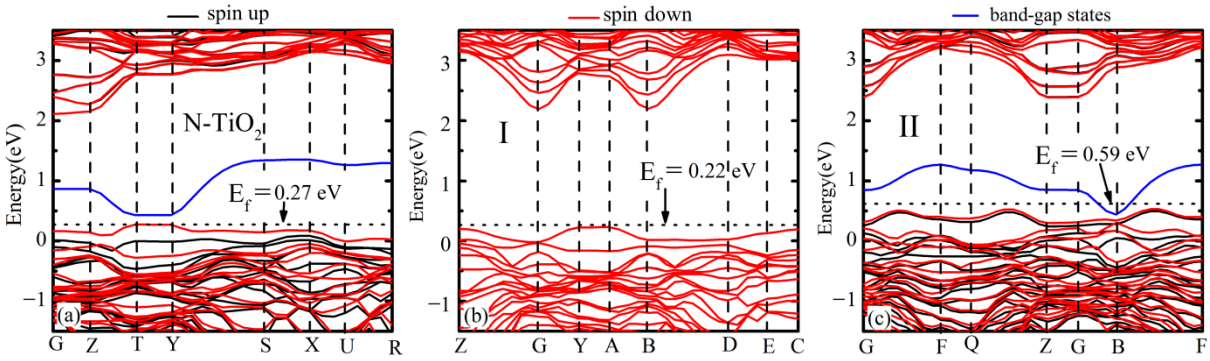


Figure 2. Band structures for (**a**) N-TiO_2, (**b**) sample I, and (**c**) sample II. The highest occupied level is chosen as the Fermi level E_f indicated with dotted line, and the E_f of TiO_2 is used as the reference level which is set to 0 eV. This reference level is also employed in Figures 3 and 4.

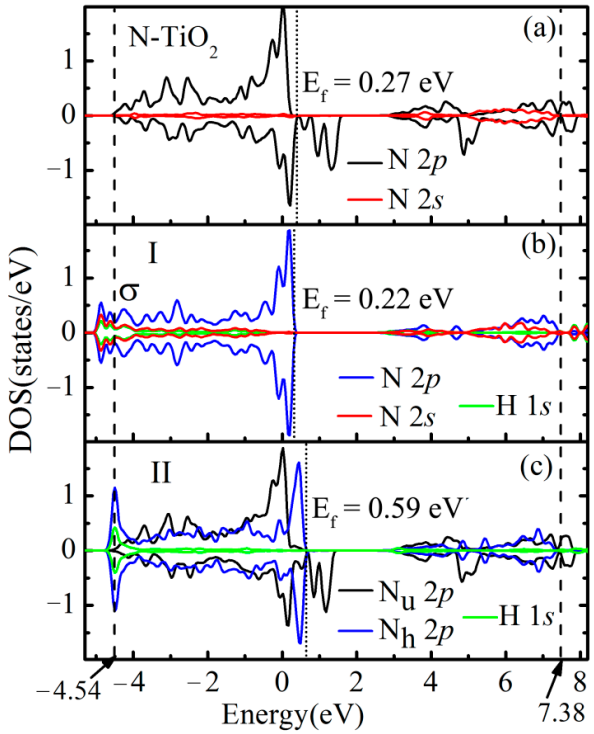


Figure 3. PDOS of N and H atoms in (**a**) N-TiO_2, (**b**) sample I, and (**c**) sample II. PDOS of N 2*s* are enlarged three times for clarity.

For sample II (see Figures 2c and 4c), the band-gap states retain the spreading characteristics, which are composed of N_u 2*p*, O 2*p* and Ti 3*d* states and originated from spin-down accepter states. This is very similar to the case in N-TiO_2 (see Figure 4a). However, the VBM remarkably move to a higher energy by 0.59 eV, and the intensity of DOS near VB edge is significantly greater than that in the N-TiO_2 system (see Figure 4a,c). Accordingly, compared to N-TiO_2, the distance between VBM and band-gap states is pulled in, resulting in a great reduction of E_g, and these band-gap states become shallower acceptor states. The significantly narrowed E_g and the shallower acceptor states can increase the light response range, which were supported by experimental observation [29]. Furthermore, the shallower acceptor states also could act as electron trapping centers, believably promoting photogenerated electron-hole separation in space [38,39]. In addition, the electron leap from VB to CB in each system is indirect (as shown in Figures 2 and S2). However, the electrons jump from VB to the band-gap states of N-TiO_2 is different from that of sample II. In N-TiO_2, the VBM and the bottom of impurity band in band gap at the same point. While

in sample II, the VBM is higher than the top valence bands at B point, and the electrons could leap directly from VB to the band-gap states at B point, and then the holes move from the B point to the VBM, realizing the separation of photogenerated electron-hole pairs. Accordingly, the diffusion length and reaction time of the electron and hole excited increase in sample II. Furthermore, the impurity band in the band gap of sample II has a higher dispersion compared to N-TiO_2, because the impurity band of N-TiO_2 exhibits a flattened shape in some high symmetry directions of the reciprocal space. Therefore, partially hydrogenated N doping can improve the VL photocatalytic activity of TiO_2.

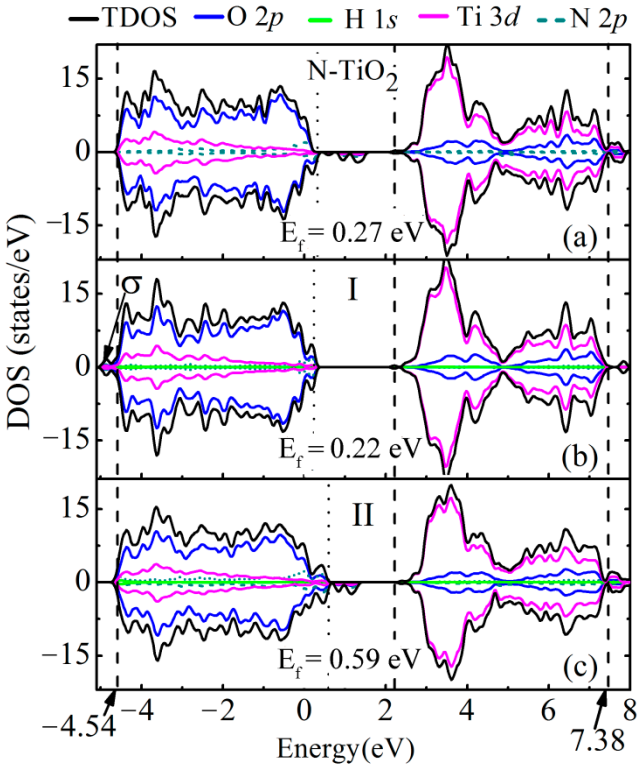


Figure 4. TDOS and PDOS for (**a**) N-TiO_2, (**b**) sample I, and (**c**) sample II.

Based on the optimized structure of sample II, the N dopant atom is located within a tetrahedron composed of H and three near-neighboring Ti atoms, and we speculate that hydrogenation enhances the 2*s*-2*p* hybridization of N, which in turn forms stronger chemical bonds with the surrounding cations. To prove this speculation, the PDOS of N 2*s* and 2*p* for N-TiO_2 and sample I were analyzed. Furthermore, since H bonding with N plays an important role in system stability, the PDOS of H 1*s* were examined in hydrogenated systems as well. As displayed in Figure 3a, the density of N 2*p* states in spin-up channel is different from that in spin-down channel for N-TiO_2, and there are some empty band-gap states ranging from 0.43 to 1.35 eV. For sample I, the band-gap states disappear, and the spin-up PDOS spectra is the same as the spin-down spectra (see Figure 3b). The H 1*s* states occur around −4.54 eV and have a strong coupling with N 2*p* and 2s states to form the N–H bond. In comparison with the N-TiO_2, the N 2*s* and 2*p* orbital hybridization was enhanced after H implantation.

To examine the effect of N_u and N_h interactions on the VB edge states in sample II, we analyzed the PDOS of 2*p* of N_u and N_h (see Figure 3c). In comparison with the states in sample I, the occupied N_h 2*p* states together with H 1*s* are holistically pushed to higher energy region. Their density peak near VB edge becomes lower, while the density peak near −4.54 eV becomes higher. On the other hand, compared to N-TiO_2, the density peak of occupied N_u 2*p* states near 0 eV becomes lower, and some occupied N_u 2*p* states appear at the range from 0.27 eV to 0.59 eV. In general, the interaction between N_h and N_u in sample II, shifts the occupied N (N_h and N_u) 2*p* states to higher energy region, which

makes the VBM dramatically shift to a higher energy position and deeply mix with the band-gap states.

3.3. Orbital Analysis

To further investigate the effect of the hydrogenation on the carrier transmission property of N-TiO_2, we examined the distributions of electronic states near the band edges via orbital analysis for sample I and II. The spin orbitals for the VBM and CBM of sample I are displayed in Figure 5a,b, respectively. It could be found that some VBM electron states localize at sites of N 2*p* orbitals, while the remainders disperse in regions of nonbonding O 2*p* orbitals. The distribution of the CBM is highly delocalized. These states are almost averagely distributed in the areas of nonbonding Ti 3*d* orbitals, where the nonbonding 3*d* orbitals of three Ti ions adjacent to N make a comparatively smaller contribution. For sample II, the interaction between the N_u and N_h slightly affects the distribution of electronic states near VB edges. As shown in Figure 5c, part VBM states assemble in the spaces of N_h 2*p* orbitals, while the other states distribute in the locations of N_u 2*p* and O 2*p* orbitals. The N_u 2*p* states have a less contribution to the VBM than N_h 2*p* states. As illustrated in Figure 5d, the orbitals related to band-gap states are mainly made of the 2*p* states of N_u atom, while the 2*p* states of O atom next to N_u also makes a tiny contribution to it. It is noted that the orbital distributions of band-gap states changes a little compared to that of N-TiO_2 (see Figure 2 in [25]). The states for the CBM, as plotted in Figure 5e, are mainly diffused around the Ti atoms far from the N_h and N_u atoms, which is similar to the situation of sample I (see Figure 5b). Thus, we can conclude that the electron mobility in CBs is almost unaffected by the H incorporating, while the synergistic effects of N_u and N_h will optimize the hole transport by delocalizing the VB edge states.

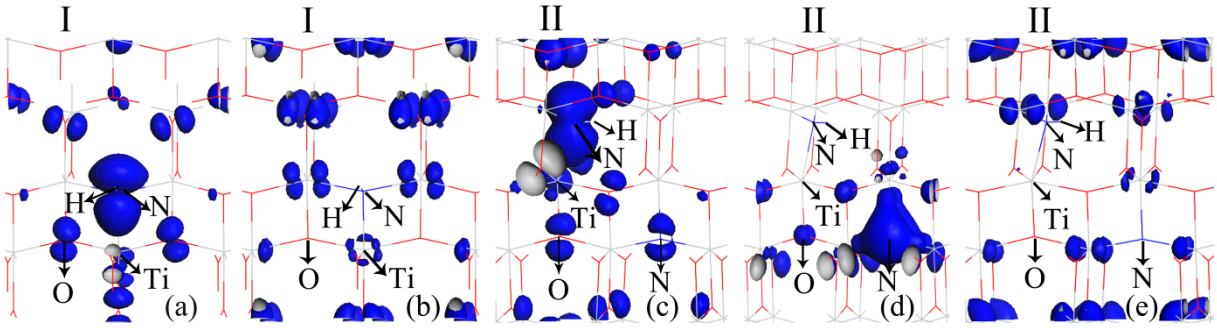


Figure 5. The isosurfaces of spin orbitals for the bands of (**a**) VBM and (**b**) CBM of sample I; (**c**) VBM, (**d**) band-gap states, and (**e**) CBM of sample II. The atomic positions of H, N, O, and Ti are indicated. The isosurface value is set to 0.015 $e/Å^3$.

3.4. Mulliken Population Analysis

Mulliken population analysis could help to further reveal the origin of the electronic structure changes of N-TiO_2 induced by hydrogenation. The calculated data of all ions in N-TiO_2, sample I, and sample II are listed in Table 2. In N-TiO_2, the charges on N are −0.58 *e*, while the charges on the O ions in the O–Ti–N chain are varied from −0.68 *e* to −0.66 *e*. Among the three Ti atoms nearest to the doped N atom, two Ti have the net charge of +1.29 *e*, and the other one has the net charge of +1.31 *e*. After N bonded to H, the charges on N are noticeably increased to −0.86, and the H has the charges of +0.26 *e* in sample I. In addition, only the net charge number of some ions in the N–Ti–O chain changes slightly, e.g., from −0.67 *e* to −0.66 *e* for O atoms and from +1.33 *e* to +1.32 *e* for Ti atoms. In this system, the quantities of ions with unchanged net charge is five for Ti and nine for O, while there are four Ti ions and seven O ions whose net charges are unaffected in N-TiO_2. Hence, the number of ions affected by the hydrogenated N decreases. Moreover, compared with the case of TiO_2, the net charge of these affected ions in sample I does not change significantly (less than 0.01 *e*). In sample II, the net charges on H ions are still +0.26 *e* but

the ones on N_h are reduced to −0.84, and the ones on N_u increase to −0.59 *e*. Additionally, there are only two Ti and two O ions with the unchanged net charges. Lots of O and Ti ions adjust their gain and loss of electrons, such as the charges on O are ranging from −0.65 to −0.68 and the ones on Ti are varied from +1.28 to +1.33. From these data, we learn that, the N_u and N_h can not only influence each other, but affect most of other ions through electron transfer.

Table 2. Net charges on all ions in N-TiO_2, sample I, and sample II obtained through Mulliken population analysis. Positive (+) and negative (−) signs mean the loss and gain of electron, respectively. The numbers in parentheses represent the quantity of ions.

System	Ti	O	N_u	N_h	H
N-TiO_2	+1.33 (4) +1.29 (2) +1.32 (1) +1.31 (1)	−0.67 (7) −0.66 (7) −0.68 (1)	−0.58	-	-
sample I	+1.33 (5) +1.32 (3)	−0.67 (9) −0.66 (6)	-	−0.86	+0.26
sample II	+1.33 (2) +1.32 (1) +1.30 (2) +1.31 (1) +1.29 (1) +1.28 (1)	−0.67 (2) −0.66 (8) −0.68 (3) −0.65 (1)	−0.59	−0.84	+0.26

3.5. Optical Properties

As mentioned above, partially hydrogenation could narrow the band-gap of N-TiO_2, hopefully improving its light absorption. To verify this speculation, here we explore the optical properties for all these three samples (N-TiO_2, sample I, and sample II) by considering the imaginary part of the dielectric function (ε_2) and absorption spectra. For a better comparison, we also considered the case of TiO_2.

It is well known that, ε_2 can directly reflect the probability that electrons absorb the energy of incident photons and then electrons jump from occupied states to unoccupied states [41]. According to Figure 6a, we can see that, for the N-TiO_2, sample I, and sample II, the ε_2 extend to low energy region with the order of sample I < N-TiO_2 < sample II, consistent with the order of the variation of E_g for them. The maximum value of ε_2 for sample II is slightly larger than that of ε_2 for N-TiO_2. Additionally, in TiO_2 and sample I, there is only one intrinsic absorption peak originating from the electron transfer from VB to CB. For N-TiO_2 and sample II, besides the intrinsic absorption peak, there is an extrinsic peak, which comes from the transition of electrons from VB to band-gap states. In N-TiO_2, the extrinsic peak appears at about 1.35 eV, where the maximum value of the ε_2 is 1.50. While the extrinsic peak occurs at about 0.55 eV, and the maximum value of the ε_2 is 6.90 in sample II, due to the significantly elevated VBM and the larger intensity of DOS near VB edge. The significantly higher VBM scales down the energy required for the electron jump from the valence band to the band-gap states, resulting in the appearance of the extrinsic peak at a lower energy position. While the larger DOS intensity near the VB edge provides a relatively sufficient transition electrons from the VB to the band-gap states, leading to a higher maximum value of the ε_2. This directly demonstrates that the band-gap state energy levels in sample II are shallower than that in N-TiO_2, and due to the lower transition energy needed, the electrons jump from VB to band-gap states more easily, giving rise to a relatively higher photoexcited carrier concentration under solar irradiation. In addition, the shallower acceptor states not only serve as a bridge for electron transition from VB to CB, extending the photoresponse range, but also improve the electron-hole separation.

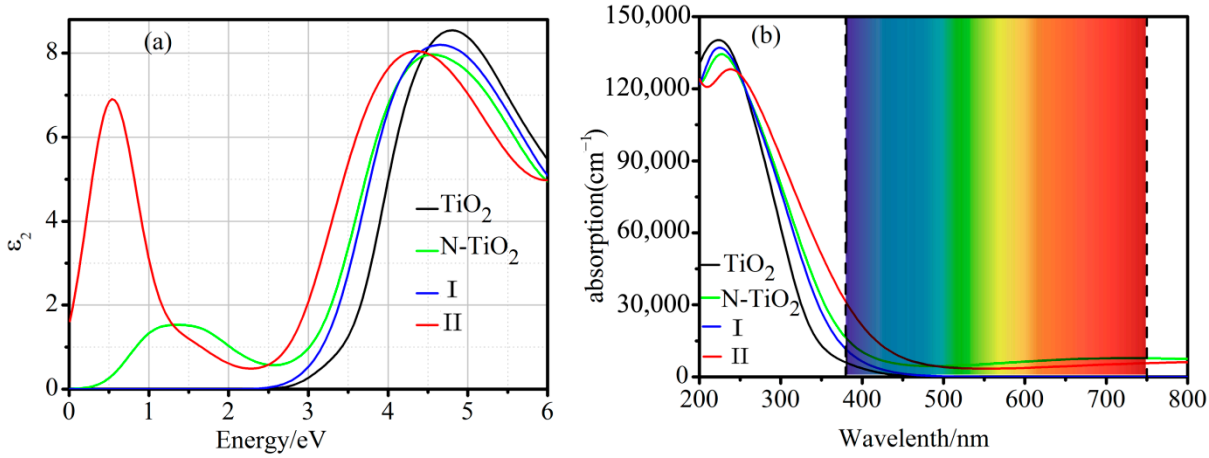


Figure 6. (**a**) The calculated imaginary part of dielectric function, and (**b**) optical absorption for TiO_2, N-TiO_2, sample I, and sample II.

As displayed in Figure 6b, compared to TiO_2, sample I shows a slight red shift in optical absorption edge, due to the tiny reduction of E_g. However, compared with N-TiO_2, its light absorption range is reduced, ascribe to the completely hydrogenation which enlarges the E_g of N-TiO_2. For sample II, the absorption edge extends to about 475 nm, showing a clear redshift of the optical absorption edge. Furthermore, for N-TiO_2 and sample II, they all have absorption in the IR region due to electron transfer from VB to band-gap states (see Figure S4). However, sample II shows higher absorption intensity and wider absorption range in the IR region compared to N-TiO_2. The change of optical absorption edge for all systems is consistent with the energy band diagrams in Figure 2, which is in agreement with the experimentally observed absorption edge shift of TiO_2 films synthesized in different atmospheres [29]. By comparison, the partially hydrogenated N doping can not only extend the solar light absorption edge towards the VL area, but also greatly enhance the VL absorption. Therefore, partially hydrogenation is a promising approach to enhance the photocatalytic activity of N-TiO_2 by improving the utilization ratio of solar energy.

3.6. Mechanism of Electronic Structure Change

The mechanism of electronic structure change in the hydrogenated N-TiO_2 can be explained as follows. When the N is bonded to H, there are no unpaired electrons in sample I, and the band-gap states disappear. In this chemical environment, N 2*s* orbitals recombine with N 2*p* orbitals to generate new hybridized orbitals. The new hybridized orbitals are all easily overlapped with Ti 3*d* and H 1*s* orbitals to form stronger N–Ti and N–H bonds, which improve the σ bonding states (see Figure 3b). As a result, the local structures adjacent to N are distorted to some extent, and the stability of the sample I increases. The confinement of the stronger bond orbitals making the bonding electrons influence on the other ions weaker, the VBM is decreased compared to N-TiO_2 (see Figure 7). Furthermore, the strong attraction between N core and H proton decreases the N–H bonding electronic energy level, and makes the N–H bonding states appear at lower energy region in VBs (see Figure 3b). In sample II, the overlap of N_u 2*p* orbitals with N_h 2*p* is larger than that of N 2*p* with O 2*p* in N-TiO_2 under the same conditions, because 2*p* orbital of N_u and N_h have the similar energy levels (see Figure 7). Furthermore, the comparatively stronger delocalized unpaired electron enhances the interaction between N_u and N_h through the electron transferring among the ions, raising the energy levels of N_h 2*p* orbital (see Figure 7), as well as some O 2*p* and Ti 3*d* orbitals (see Figure 4c). Accordingly, the VBM is raised substantially and the intensity of the DOS near the VB edge becomes greater in comparation with that of N-TiO_2.

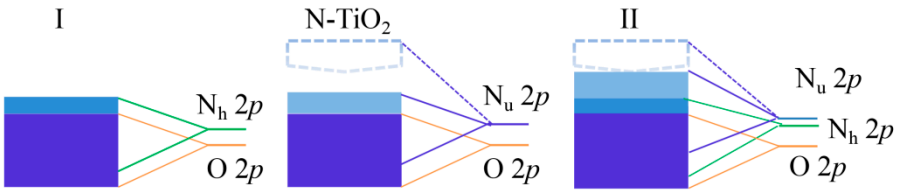


Figure 7. Schematic diagram of the change of valence band edges for N-TiO_2, sample I, and sample II. Different shades of blue represent the intensity of the electron density. The darker color stands for the greater electronic density. The blank area of the short dashed line box represents the band-gap states.

3.7. Photocatalytic Property

In order to give a clear explanation for the effect of partially hydrogenation on the photocatalytic activity of N-TiO_2, the schematic diagram of the mechanism of VL photocatalytic hydrogen generation from water splitting is provided in Figure 8. The synergistic effect of N_u and N_h significantly shifts up the energy of VBM, narrows the E_g, and delocalize the high energy electron states near VB edge, which have definitive influence on its VL absorption and photocatalytic performance. The remarkably lifted VBM mixing with the broadening band-gap states serves to promote the electron excitation from VB states to the band-gap states (see Figure 6a) and then to CB states by absorbing VL (see Figures 6b and 8). Additionally, the delocalization of high energy electrons near VB edge with the wide band-gap states facilitates the separation of electron-hole pairs and increases the transport of photogenerated carriers to photocatalyst surface. The photogenerated electrons transferred to the surface reduce water to produce hydrogen, and the photogenerated holes transferred to the surface oxidize water to generate oxygen. Hence, the enhanced efficiency of carrier transition improve the VL photocatalytic activity of sample II. In this way, we can clearly understand the reasons why the N-TiO_2 with H incorporation possesses higher VL photocatalytic activity than N-TiO_2 [28].

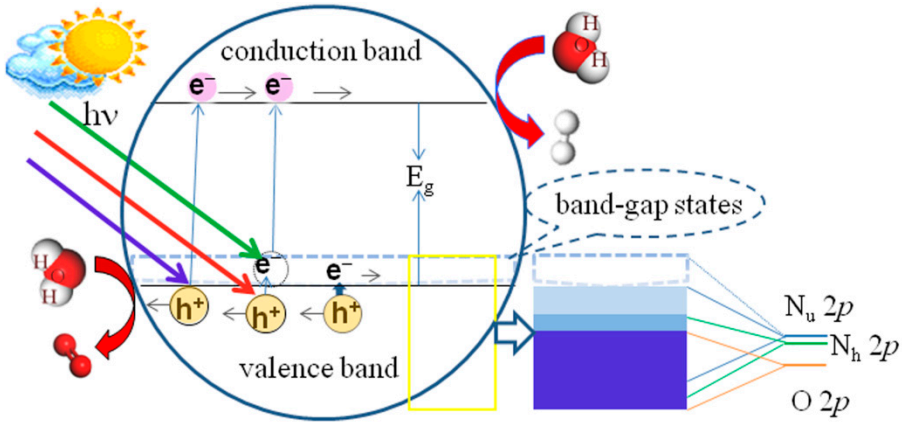


Figure 8. Schematic diagram of the mechanism of photocatalytic hydrogen production from water splitting by sample II using sun light.

4. Conclusions

In summary, completely and partially hydrogenated N-TiO_2 are systematically investigated by the spin-polarized DFT calculations. The calculated results demonstrate that, with respect to N-TiO_2, both the hydrogenated samples are energetically favorable under Ti-rich conditions. For completely hydrogenated N-TiO_2, the band-gap states disappear and the E_g becomes a little larger (about 0.05 eV). As to the partially hydrogenated N-TiO_2, the stronger interaction between N_h and N_u dramatically makes the VBM move to higher energy by 0.32 eV and increases the intensity of DOS near the VBM. The shift of VBM closes the distance between the band-gap states and VBM and forms the shallower acceptor states. The largely E_g reduction and the shallower acceptor states extend the light response range. Furthermore, the shallower acceptor states also serve to separate the photogenerated

electron-hole pairs. Therefore, partially hydrogenation is able to further improve the VL photocatalytic activity of N-TiO_2. Our findings provide a rational interpretation for the experimental observation of enhanced VL photocatalytic performance of N-TiO_2 specimen with H incorporation, and suggest an avenue to improve catalytic activity for efficient photocatalytic water-splitting reaction.

Supplementary Materials: The following supporting information can be downloaded at: https://www.mdpi.com/article/10.3390/catal12020178/s1, Figure S1: The atomic structures of the H–O configurations; Figure S2: Band structure for TiO_2; Figure S3: TDOS and PDOS for TiO_2; Figure S4: The optical absorption for N-TiO_2 and sample II in visible light and IR region; Table S1: The calculated lattice parameters for N-TiO_2; Table S2: Formation energies (E_{form}, in eV) for H–O and H–Ti configurations under various growth conditions.

Author Contributions: Data curation, D.Z.; Formal analysis, D.Z., X.T., D.Y. and L.J.; Funding acquisition, L.J.; Investigation, X.Q. and Z.T.; Project administration, L.J.; Software, Z.T.; Supervision, L.J.; Writing—original draft, D.Z., D.Y. and L.J. All authors have read and agreed to the published version of the manuscript.

Funding: This research was funded by National Natural Science foundation of China (Grants No. 11804006), the Henan Scientific Research Fund for Returned Scholars, Henan Key Program of Technology Research and Development (No. 202102210200), the Foundation for University Youth Key Teacher by the Henan Province (Grant No. 2019GGJS190), and the Research Incubation Fund of Anyang Normal University (No. AYNUKP-2017-A06).

Data Availability Statement: The data presented in this study are available in Supplementary Materials.

Acknowledgments: L.J. thanks Mingyan Chen (from HZWTECH) for help and discussions regarding this study.

Conflicts of Interest: The authors declare no conflict of interest.

References

1. Fujishima, A.; Honda, K. Electrochemical Photolysis of Water at a Semiconductor Electrode. *Nature* **1972**, *238*, 37–38. [CrossRef] [PubMed]
2. Takata, T.; Jiang, J.; Sakata, Y.; Nakabayashi, M.; Shibata, N.; Nandal, V.; Seki, K.; Hisatomi, T.; Domen, K. Photocatalytic water splitting with a quantum efficiency of almost unity. *Nature* **2020**, *581*, 411–414. [CrossRef] [PubMed]
3. Ju, L.; Shang, J.; Tang, X.; Kou, L. Tunable Photocatalytic Water Splitting by the Ferroelectric Switch in a 2D AgBiP2Se6 Monolayer. *J. Am. Chem. Soc.* **2020**, *142*, 1492–1500. [CrossRef] [PubMed]
4. Ju, L.; Qin, J.; Shi, L.; Yang, G.; Zhang, J.; Sun, L. Rolling the WSSe Bilayer into Double-Walled Nanotube for the Enhanced Photocatalytic Water-Splitting Performance. *Nanomaterials* **2021**, *11*, 705. [CrossRef]
5. Cai, J.; Shen, J.; Zhang, X.; Ng, Y.H.; Huang, J.; Guo, W.; Lin, C.; Lai, Y. Light-Driven Sustainable Hydrogen Production Utilizing TiO_2 Nanostructures: A Review. *Small Methods* **2019**, *3*, 1800184. [CrossRef]
6. Ju, L.; Liu, P.; Yang, Y.; Shi, L.; Yang, G.; Sun, L. Tuning the photocatalytic water-splitting performance with the adjustment of diameter in an armchair WSSe nanotube. *J. Energy Chem.* **2021**, *61*, 228–235. [CrossRef]
7. Singh, R.; Dutta, S. A review on H2 production through photocatalytic reactions using TiO_2/TiO_2-assisted catalysts. *Fuel* **2018**, *220*, 607–620. [CrossRef]
8. Kumaravel, V.; Mathew, S.; Bartlett, J.; Pillai, S.C. Photocatalytic hydrogen production using metal doped TiO_2: A review of recent advances. *Appl. Catal. B Environ.* **2019**, *244*, 1021–1064. [CrossRef]
9. Suwannaruang, T.; Kidkhunthod, P.; Chanlek, N.; Soontaranon, S.; Wantala, K. High anatase purity of nitrogen-doped TiO_2 nanorice particles for the photocatalytic treatment activity of pharmaceutical wastewater. *Appl. Surf. Sci.* **2019**, *478*, 1–14. [CrossRef]
10. Zhang, J.; Zhou, P.; Liu, J.; Yu, J. New understanding of the difference of photocatalytic activity among anatase, rutile and brookite TiO_2. *Phys. Chem. Chem. Phys.* **2014**, *16*, 20382–20386. [CrossRef]
11. Khan, M.; Yi, Z.; Fawad, U.; Muhammad, W.; Niaz, A.; Zaman, M.I.; Ullah, A. Enhancing the photoactivity of TiO_2 by codoping with silver and molybdenum: The effect of dopant concentration on the photoelectrochemical properties. *Mater. Res. Express* **2017**, *4*, 045023. [CrossRef]
12. Chen, X.; Liu, L.; Yu, P.Y.; Mao Samuel, S. Increasing Solar Absorption for Photocatalysis with Black Hydrogenated Titanium Dioxide Nanocrystals. *Science* **2011**, *331*, 746–750. [CrossRef] [PubMed]
13. Liu, B.; Zhao, X. The synergetic effect of V and Fe-co-doping in TiO_2 studied from the DFT + U first-principle calculation. *Appl. Surf. Sci.* **2017**, *399*, 654–662. [CrossRef]

14. Niu, M.; Zhang, J.; Cao, D. I, N-Codoping Modification of TiO_2 for Enhanced Photoelectrochemical H_2O Splitting in Visible-Light Region. *J. Phys. Chem. C* **2017**, *121*, 26202–26208. [CrossRef]
15. Wang, D.; Zheng, Y.; Tian, J.; Jing, T.; Kan, W.; Hu, Y. Theoretical calculation and experiment study on the electronic structure, microstructures and photocatalytic activity of N–Al codoped TiO_2. *RSC Adv.* **2017**, *7*, 52105–52110. [CrossRef]
16. Zhao, Y.; Wang, W.; Li, C.; He, L. Electronic and photocatalytic properties of N/F co-doped anatase TiO_2. *RSC Adv.* **2017**, *7*, 55282–55287. [CrossRef]
17. Zhao, W.; Liu, S.; Zhang, S.; Wang, R.; Wang, K. Preparation and visible-light photocatalytic activity of N-doped TiO_2 by plasma-assisted sol-gel method. *Catal. Today* **2019**, *337*, 37–43. [CrossRef]
18. Avilés-García, O.; Espino-Valencia, J.; Romero-Romero, R.; Rico-Cerda, J.L.; Arroyo-Albiter, M.; Solís-Casados, D.A.; Natividad-Rangel, R. Enhanced Photocatalytic Activity of Titania by Co-Doping with Mo and W. *Catalysts* **2018**, *8*, 631. [CrossRef]
19. Piątkowska, A.; Janus, M.; Szymański, K.; Mozia, S. C-,N- and S-Doped TiO_2 Photocatalysts: A Review. *Catalysts* **2021**, *11*, 144. [CrossRef]
20. Assadi, M.H.N.; Hanaor, D.A. The effects of copper doping on photocatalytic activity at (101) planes of anatase TiO_2: A theoretical study. *Appl. Surf. Sci.* **2016**, *387*, 682–689. [CrossRef]
21. Khaselev, O.; Turner John, A. A Monolithic Photovoltaic-Photoelectrochemical Device for Hydrogen Production via Water Splitting. *Science* **1998**, *280*, 425–427. [CrossRef] [PubMed]
22. Gai, Y.; Li, J.; Li, S.-S.; Xia, J.-B.; Wei, S.-H. Design of Narrow-Gap TiO_2: A Passivated Codoping Approach for Enhanced Photoelectrochemical Activity. *Phys. Rev. Lett.* **2009**, *102*, 036402. [CrossRef] [PubMed]
23. Asahi, R.; Morikawa, T.; Ohwaki, T.; Aoki, K.; Taga, Y. Visible-Light Photocatalysis in Nitrogen-Doped Titanium Oxides. *Science* **2001**, *293*, 269–271. [CrossRef] [PubMed]
24. Irie, H.; Watanabe, Y.; Hashimoto, K. Nitrogen-Concentration Dependence on Photocatalytic Activity of TiO_2-xNx Powders. *J. Phys. Chem. B* **2003**, *107*, 5483–5486. [CrossRef]
25. Zhao, D.; Huang, X.; Tian, B.; Zhou, S.; Li, Y.; Du, Z. The effect of electronegative difference on the electronic structure and visible light photocatalytic activity of N-doped anatase TiO_2 by first-principles calculations. *Appl. Phys. Lett.* **2011**, *98*, 162107. [CrossRef]
26. Yang, K.; Dai, Y.; Huang, B. Study of the Nitrogen Concentration Influence on N-Doped TiO_2 Anatase from First-Principles Calculations. *J. Phys. Chem. C* **2007**, *111*, 12086–12090. [CrossRef]
27. Esmat, M.; El-Hosainy, H.; Tahawy, R.; Jevasuwan, W.; Tsunoji, N.; Fukata, N.; Ide, Y. Nitrogen doping-mediated oxygen vacancies enhancing co-catalyst-free solar photocatalytic H2 production activity in anatase TiO_2 nanosheet assembly. *Appl. Catal. B Environ.* **2021**, *285*, 119755. [CrossRef]
28. Mi, L.; Xu, P.; Shen, H.; Wang, P.-N.; Shen, W. First-principles calculation of N:H codoping effect on energy gap narrowing of TiO_2. *Appl. Phys. Lett.* **2007**, *90*, 171909. [CrossRef]
29. Xu, P.; Mi, L.; Wang, P.-N. Improved optical response for N-doped anatase TiO_2 films prepared by pulsed laser deposition in $N_2/NH_3/O_2$ mixture. *J. Cryst. Growth* **2006**, *289*, 433–439. [CrossRef]
30. Mi, L.; Zhang, Y.; Wang, P.-N. First-principles study of the hydrogen doping influence on the geometric and electronic structures of N-doped TiO_2. *Chem. Phys. Lett.* **2008**, *458*, 341–345. [CrossRef]
31. Pan, H.; Zhang, Y.-W.; Shenoy, V.B.; Gao, H. Effects of H-, N-, and (H, N)-Doping on the Photocatalytic Activity of TiO_2. *J. Phys. Chem. C* **2011**, *115*, 12224–12231. [CrossRef]
32. Li, M.; Zhang, J.; Guo, D.; Zhang, Y. Band gap engineering of compensated (N, H) and (C, 2H) codoped anatase TiO_2: A first-principles calculation. *Chem. Phys. Lett.* **2012**, *539–540*, 175–179. [CrossRef]
33. Russo, S.P.; Grey, I.E.; Wilson, N.C. Nitrogen/Hydrogen Codoping of Anatase: A DFT Study. *J. Phys. Chem. C* **2008**, *112*, 7653–7664. [CrossRef]
34. Hongzhiwei Technology, D.S. Version 2021A, China. Available online: https://iresearch.net.cn/cloudSoftware (accessed on 1 November 2021).
35. Segall, M.D.; Lindan, P.J.D.; Probert, M.; Pickard, C.J.; Hasnip, P.; Clark, S.; Payne, M.C. First-principles simulation: Ideas, illustrations and the CASTEP code. *J. Phys. Condens. Matter* **2002**, *14*, 2717–2744. [CrossRef]
36. Monkhorst, H.J.; Pack, J.D. Special points for Brillouin-zone integrations. *Phys. Rev. B* **1976**, *13*, 5188–5192. [CrossRef]
37. Shi, A.J.; Li, B.X.; Wan, C.R.; Leng, D.C.; Lei, E.Y. Hybrid density functional studies of C-anion-doped anatase TiO_2. *Chem. Phys. Lett.* **2016**, *650*, 19–28. [CrossRef]
38. Bagwasi, S.; Tian, B.; Zhang, J.; Nasir, M. Synthesis, characterization and application of bismuth and boron Co-doped TiO_2: A visible light active photocatalyst. *Chem. Eng. J.* **2013**, *217*, 108–118. [CrossRef]
39. Ibrahim, H.H.; Mohamed, A.A.; Ibrahim, I.A. Electronic and optical properties of mono and co-doped anatase TiO_2: First principles calculations. *Mater. Chem. Phys.* **2020**, *252*, 123285. [CrossRef]
40. Doustkhah, E.; Assadi, M.H.N.; Komaguchi, K.; Tsunoji, N.; Esmat, M.; Fukata, N.; Tomita, O.; Abe, R.; Ohtani, B.; Ide, Y. In situ Blue titania via band shape engineering for exceptional solar H_2 production in rutile TiO_2. *Appl. Catal. B Environ.* **2021**, *297*, 120380. [CrossRef]
41. Zhu, H.X.; Liu, J.-M. First principles calculations of electronic and optical properties of Mo and C co-doped anatase TiO_2. *Appl. Phys. A* **2014**, *117*, 831–839. [CrossRef]